• Basic Research •

# Prognostic prediction model for Chinese uveal melanoma patients based on matrix metalloproteinase-2 and -28 expression levels in the tumor

*Yu-Ning Chen[1], Jing-Ying Xiu[1], Han-Qing Zhao[1], Jing-Ting Luo[1], Qiong Yang[1], Yang Li[1,2], Wen-Bin Wei[1]*

[1]Beijing Tongren Eye Center, Beijing Key Laboratory of Intraocular Tumor Diagnosis and Treatment, Beijing Ophthalmology & Visual Sciences Key Lab, Medical Artificial Intelligence Research and Verification Key Laboratory of the Ministry of Industry and Information Technology, Beijing Key Laboratory of Intelligent Diagnosis, Treatment and Prevention of Blinding Eye Diseases, Beijing Tongren Hospital, Capital Medical University, Beijing 100730, China
[2]Beijing Institute of Ophthalmology, Beijing Tongren Hospital, Capital Medical University, Beijing 100005, China
**Co-first Authors:** Yu-Ning Chen and Jing-Ying Xiu
**Correspondence to:** Wen-Bin Wei. Beijing Tongren Eye Center, Beijing Key Laboratory of Intraocular Tumor Diagnosis and Treatment, Beijing Ophthalmology & Visual Sciences Key Lab, Medical Artificial Intelligence Research and Verification Key Laboratory of the Ministry of Industry and Information Technology, Beijing Tongren Hospital, Capital Medical University, Beijing 100730, China. weiwenbintr@163.com; Yang Li. Beijing Tongren Eye Center, Beijing Key Laboratory of Intraocular Tumor Diagnosis and Treatment, Beijing Ophthalmology & Visual Sciences Key Lab, Medical Artificial Intelligence Research and Verification Key Laboratory of the Ministry of Industry and Information Technology; Beijing Institute of Ophthalmology, Beijing Tongren Hospital, Capital Medical University, Beijing 100005, China. liyangtongren@163.com
Received: 2025-02-07 Accepted: 2025-02-25

## Abstract

● **AIM:** To explore the relationship between matrix metalloproteinases (MMPs) expression levels in the tumor and the prognosis of uveal melanoma (UM) and to construct prognostic prediction models.

● **METHODS:** Transcriptome sequencing data from 17 normal choroid tissues and 53 UM tumor tissues were collected. Based on the differential gene expression levels and their function, MMPs family was selected for establishing risk-score system and prognostic prediction model with machine learning. Tumor microenvironment (TME) analysis was also applied for the impact of immune cell infiltration on prognosis of the disease.

● **RESULTS:** Eight MMPs were significantly different expression levels between normal and the tumor tissues. MMP-2 and MMP-28 were selected to construct a risk-score system and divided patients accordingly into high- and low-risk groups. The prediction model based on the risk-score achieved an accuracy of approximately 80% at 1-, 3-, and 5-year after diagnosis. Besides, a Nomogram prognostic prediction model which based on risk-score and pathological type (independent prognostic factors after Cox regression analysis) demonstrated good consistency between the predicted outcomes at 1-, 3-, and 5-year after diagnosis and the actual prognosis of patients. TME analysis revealed that the high-risk group exhibited higher immune and stromal scores and increased infiltration of tumor-associated macrophages (TAMs) and regulatory T cells compared to the low-risk group.

● **CONCLUSION:** Based on MMP-2 and MMP-28 expression levels, our prediction model demonstrates accurate long-term prognosis prediction for UM patients. The aggregation of TAMs and regulatory T cells in the TME of UM may be associated with an unfavorable prognosis.

● **KEYWORDS:** uveal melanoma; matrix metalloproteinases; prediction model; prognosis; tumor microenvironment
**DOI:10.18240/ijo.2025.05.02**

**Citation:** Chen YN, Xiu JY, Zhao HQ, Luo JT, Yang Q, Li Y, Wei WB. Prognostic prediction model for Chinese uveal melanoma patients based on matrix metalloproteinase-2 and -28 expression levels in the tumor. *Int J Ophthalmol* 2025;18(5):765-778

## INTRODUCTION

Uveal melanoma (UM) is the most common primary malignant ocular tumor in adults. The incidence of UM in Europe and the United States is about 5/1 000 000 annually[1], while the incidence of Asian[2] is 0.6/1 000 000,

significantly lower than that in Western. The main treatments of UM nowadays are radiotherapy and enucleation. In addition, local resection and laser therapy have also been applied in UM. Researchers have found that the mortality rates of patients treated with local radiation therapy[3], local resection[4], and enucleation are similar. As an intraocular tumor with an extremely high malignancy, nearly half of UM patients eventually experience metastasis. Tumor cells primarily metastasize through hematogenous spread, with the liver being the most common site. It has been found that many patients have already metastasized before treatment, and most patients die quickly after metastasis[5]. Therefore, how to predict UM metastasis and death outcomes in the early stage has become a highly concerned and urgent issue for clinical doctors.

Matrix metalloproteinases (MMPs) are a family of zinc-dependent endopeptidases, serving as the primary proteases responsible for the degradation of the extracellular matrix (ECM) and basement membrane. Functioning as crucial hydrolytic enzymes, MMPs play a role in regulating the degradation and remodeling of the ECM, thereby participating not only in normal physiological processes but also playing a significant role in the occurrence and development of tumors. Previous studies have indicated that various cell types within tumor cells and tumor microenvironment (TME), such as macrophages and vascular endothelial cells, can secrete different types of MMPs. In the TME of multiple tumors, MMPs promote tumor invasion and distant metastasis through ECM degradation, facilitation of epithelial-mesenchymal transition (EMT), and stimulation of vascular endothelial growth factor secretion to induce angiogenesis[6].

TME plays a crucial role in the development, invasion, and treatment of cancer[7]. Immune checkpoint inhibitors can disrupt the inhibitory effect of tumor cells on immune cells, activate the functions of immune cells, and thus contribute to the destruction of cancer cells. Unlike the favorable treatment outcomes observed in cutaneous melanoma, UM does not respond well to some commonly used immune checkpoint inhibitors, such as anti-programmed cell death protein 1 (PD-1) and anti-cytotoxic T-lymphocyte-associated antigen 4 (CTLA-4)[8]. Therefore, many researchers also hope to explore treatment approaches for UM from other perspectives by exploring TME.

Although there have been some studies on the role of MMPs in UM, most of them are based on qualitative or semi-quantitative methods such as immunohistochemistry[9] and lack comparisons with a large amount of normal choroid tissue[10]. Therefore, this study is based on next-generation sequencing technology to compare normal choroid with UM. By integrating clinical characteristics and follow-up results, we established UM prognostic prediction models based on the MMPs family and analyzed the TME of UM, which intended to support personalized diagnosis and treatment strategies for UM patients.

## PARTICIPANTS AND METHODS

**Ethical Approval** This study adheres to the Helsinki Declaration and has received approval from the Ethics Committee of Beijing Tongren Hospital (Ethics Review Number: TRECKY2018-056). All patients provided informed consent to participate in the study.

**Clinical Tissue Sample and Participant Information Collection** Seventeen samples of normal choroid tissue were preserved at the Beijing Tongren Eye Bank, affiliated Beijing Tongren Hospital of Capital Medical University. Fifty-three samples of UM tissue were stored in the clinical database of Beijing Tongren Hospital, along with recorded clinical information and pathological data of the respective patients. All patients' diagnoses and treatment approaches were determined by the same physician (Wei WB). UM tumor tissues were obtained from local resection and enucleation procedures performed by the same physician (Wei WB), and the sample collection strictly adhered to aseptic principles.

**mRNA Data Acquisition** All 70 samples collected in this study underwent mRNA sequencing and library construction using the Novaseq6000 sequencing system. After sequencing quality checks, the expression level of mRNA was estimated using the RNA-Seq by Expectation-Maximization method. Additionally, transcriptome data and clinical information for 80 UM cases were downloaded to validate the findings from The Cancer Genome Atlas (TCGA) database (https://tcga-data.nci.nih.gov/tcga)[11].

**Differential Expression Genes and Function Analysis** The analysis of differentially expression genes (DEGs) was performed using the "limma" package[12] in R Studio (version 4.1.0). DEGs were selected from patient samples based on the criteria of $|\log_2 FC|>1$ and false discovery rate (FDR)<0.05. For the high-risk and low-risk groups, DEGs were filtered based on the criteria of $|\log_2 FC|>1$ and $P<0.05$. Then we utilized the "clusterProfiler" package[13] in R Studio to perform enrichment analysis on Gene Ontology (GO) databases (including biological process, molecular function, and cellular component) and Kyoto Encyclopedia of Genes and Genomes (KEGG) pathways. We considered entries with a $P<0.05$ as significantly enriched. Regarding the DEGs-enriched pathways in normal choroid and UM tumor tissues, we manually excluded some pathways that were evidently unrelated to tumor development. For the high- and low-risk groups, in addition to GO and KEGG enrichment, we also applied Gene Set Enrichment Analysis (GSEA) for a more comprehensive analysis of functional differences between the two groups.

**GEPIA2** GEPIA2[14] (http://gepia2.cancer-pku.cn/#general) is an online platform that analyzes and visualizes gene expression and survival data based on sequencing data from 33 cancer types in the TCGA database. It has gained recognition and citations in many articles. In this study, the survival heatmap in the TCGA database were generated by GEPIA2.

**Machine Learning Algorithm** The least absolute shrinkage and selection operator (LASSO) regression analysis was performed using the "glmnet" package[15] in R Studio to select genes associated with prognosis. Subsequently, the selected genes were used to calculate the risk-score for each tumor sample using the following formula:

$$\text{riskscore}=\sum_{i=1}^{n}\text{Coef}_i \times \text{X}_i$$

$\text{Coef}_i$ represents the coefficient of the selected gene $i$, and $\text{X}_i$ represents the expression level of the gene $i$. Patients were separated into high-risk and low-risk groups based on the median of the risk-score.

**Tumor Microenvironment Analysis** We employed the "ESTIMATE" package (https://R-Forge.R-project.org/projects/estimate/) in R Studio to estimate tumor stromal, immune components, and tumor purity score. Immune cell infiltration analysis for specific immune cells was based on CIBERSORT[16]. To analyze the differences in all-type macrophages within the TME across different risk groups, we chose the EPIC database[17] to evaluate tumor-associated macrophages (TAMs).

**Immunohistochemistry Assay** UM tissue was embedded in paraffin and affixed onto the slide. Dewaxed with xylene and graded ethanol series. Performed antigen retrieval with ethylenediaminetetraacetic acid for 30min. After depigmentation, 3% hydrogen peroxide was applied to remove endogenous peroxidase. Incubated with 3% bovine serum albumin, applied primary antibody dilution (anti-MMP2 and anti-MMP28; Proteintech Group, Inc., Wuhan, China) and secondary antibody sequentially. 3-Amino-9-ethylcarbazole and hematoxylin was used for chromogenic reaction and re-staining of nucleus. After mounting with glycerol gelatin, the results were interpreted under a bright-field microscope.

**Statistical Analysis** The "survival" package (https://CRAN.R-project.org/package=survival) and the "survminer" package (https://CRAN.R-project.org/package=survminer) were utilized to estimate survival status (both metastasis and death) for different groups by Kaplan-Meier survival analysis. The significance of survival rate differences between two risk groups was determined using two-sided Log-Rank test. Cox multivariate regression analysis was employed to identify factors significantly associated with prognosis. Due to the fact that four patients had confirmed tumor metastasis but the exact time of metastasis was uncertain, they were excluded from the metastasis-related survival analysis and Cox regression. Student's *t*-test, Chi-square test, and Fisher's exact test were applied to statistically evaluate clinical feature differences between high-risk and low-risk groups. Nomogram models are widely used for predicting the prognosis of cancer. In order to predict the survival status of patients at 1-, 3-, and 5-year after diagnosis, we utilized the "rms" package (https://cran.r-project.org/package=rms) in R Studio. We constructed a Nomogram prognostic prediction model and drew a calibration curve to observe the relationship between the Nomogram's predicted probabilities and the actual occurrence rates. All statistical analyses considered a significance level of $P<0.05$.

## RESULTS

**Clinical Information and DEGs of Chinese UM patients** We collected clinical data of all 53 Chinese UM patients (Table 1). Most patients (56.6%) were first diagnosed at 41-60 years old. The average tumor thickness was 11.2±2.6 mm and the largest basal diameter was 15.3±4.1 mm. According to the American Joint Committee on Cancer classification of UM, 66.0% of the patients were in the Stage III. The 39.6% of the tumor pathology was mixed cell-type. These results were consistent with some of the conclusions of our previous large long-term follow-up study[5]. The average follow-up time of all patients was 44.8±27.3mo.

In order to explore the genes that play an important role in the occurrence and development of UM, we sequenced the mRNA of 17 normal choroid and 53 UM samples. Compared to normal choroid tissue, there were 814 upregulated and 9172 downregulated DEGs in UM tumor tissue (Figure 1A). All DEGs were subjected to GO and KEGG enrichment analysis, revealing a significant concentration in pathways related to cell-cell interaction and ECM (Figure 1B-1C). Among the highly differentially expressed mRNAs, we observed a substantial proportion associated with the MMPs family. Previous research in cancer studies has also suggested the crucial role of MMPs in the initiation and progression of tumors[18]. Therefore, we focused on exploring the impact of MMPs on the tumor tissue of Chinese UM patients. There were 9 MMP-related DEGs, namely MMP-2, MMP-9, MMP-12, MMP-15, MMP-16, MMP-17, MMP-19, MMP-26, and MMP-28. Due to the low expression level of MMP-26, it was excluded from subsequent analyses (Figure 1D). In addition, we also analyzed the expression of the 8 MMP-related DEGs in this study across 33 types of tumors in the TCGA database and their association with prognosis. It was found that the relatively high expression of MMP-2, MMP-9, MMP-12, MMP-16, MMP-17, and MMP-28 was associated with poor prognosis of adrenocortical carcinoma, pancreatic cancer, thyroid cancer, and UM (Figure 1E). Since the majority of UM patients in TCGA are Caucasian, we aimed to investigate the

**Table 1 UM patients' clinical features and outcome** *n*=53 (%)

| Parameters | Patients |
|---|---|
| Gender | |
| Male | 26 (49.1) |
| Female | 27 (50.9) |
| Age (y) | |
| 21-40 | 14 (26.4) |
| 41-60 | 30 (56.6) |
| 61-80 | 9 (17.0) |
| Laterality | |
| Right | 27 (50.9) |
| Left | 26 (49.1) |
| Visual acuity | |
| >0.5 | 4 (7.5) |
| 0.1-0.5 | 11 (20.8) |
| <0.1 | 38 (71.7) |
| Intraocular pressure (mm Hg) | |
| 10-21 | 41 (77.4) |
| <10 | 5 (9.4) |
| >21 | 7 (13.2) |
| Thickness (mm) | |
| Median | 11.4 |
| Mean±SD | 11.2±2.6 |
| Range | 2.6-16.0 |
| Largest basal diameter (mm) | |
| Median | 15.9 |
| Mean±SD | 15.3±4.1 |
| Range | 4.1-22.5 |
| Size (T Stage)[a] | |
| T1 | 2 (3.8) |
| T2 | 2 (3.8) |
| T3 | 25 (47.2) |
| T4 | 24 (45.2) |
| Stage[a] | |
| I | 1 (1.9) |
| IIA | 2 (3.8) |
| IIB | 15 (28.3) |
| IIIA | 20 (37.7) |
| IIIB | 14 (26.4) |
| IIIC | 1 (1.9) |
| Macroscopic appearance | |
| Mushroom | 26 (49.0) |
| Hemisphere | 16 (30.2) |
| Irregular | 11 (20.8) |
| Optic disk involvement | 7 (13.2) |
| Subretinal fluid | 51 (96.2) |
| Intraocular hemorrhage | 5 (9.4) |
| Ciliary body involvement | 25 (47.2) |
| Extraocular extension | 4 (7.5) |
| Pathology | |
| Spindle cell-type | 19 (35.9) |
| Mixed cell-type | 21 (39.6) |
| Epithelioid cell-type | 13 (24.5) |
| Outcome | |
| Living without metastasis | 36 (67.9) |
| Metastasis without death | 4 (7.6) |
| Death | 13 (24.5) |
| Follow-up time (y) | |
| ≤1 | 5 (9.5) |
| >1 and ≤3 | 14 (26.5) |
| >3 and ≤5 | 26 (49.1) |
| >5 | 10 (18.9) |

[a]American Joint Committee on Cancer classification (8th edition). UM: Uveal melanoma.

relationship between the expression of MMPs and prognosis among Chinese UM patients.

**MMPs Associated with UM Clinical Features** According to previous research and clinical experience, we analyzed the differences in the expression of 8 MMP-related DEGs among the traditional prognostic risk factors. The results showed no significant difference in the expression of the 8 MMPs-related DEGs in different stages. The expression of MMP-16 being significantly higher in epithelial cell-type UM compared to mixed cell-type, while MMP-17 expression in mixed cell-type was significantly lower than in the other two pathological types (Figure 2A). As for tumor size, only MMP-2 expressed differently between T2 and T3 tumors (Figure 2B). Based on these findings, we combined follow-up data to analyze the relationship between MMPs and the actual prognosis of UM patients. We grouped all tumor samples according to the median expression of 8 MMP-related DEGs and conducted a Kaplan-Meier survival analysis for each differentially expressed MMP. The results revealed significant statistical differences in overall survival associated with the expression levels of MMP-16 and MMP-19 (Figure 2C), with MMP-16 also correlated with patients' metastasis-free survival (Figure 2D).

**Construction of MMPs-related Risk-score System** Based on the above results, we found that the expression level of MMPs is related to tumor characteristics that affect prognosis and patient survival. Therefore, we performed LASSO regression analysis on the eight differentially expressed MMPs. Based on the λ values corresponding to different numbers of genes in LASSO analysis (Figure 3A), which were MMP-2 and MMP-28, respectively. We subsequently weighted the expression levels of these two MMPs by the regression coefficients from the LASSO analysis to establish a risk-score system for predicting patient survival, where risk-score=(MMP2×0.1464 3730)+MMP28×(-0.03730257). Then, the risk-score of each patient was calculated according to the above formula, and the samples of our dataset and TCGA verification dataset were divided into high-risk group and low-risk group according to the calculated median risk-score. Clinical characteristic differences between the two groups were summarized in Table 2. Through the analysis, we found that the prognosis of the high-risk group was significantly worse than that of the low-risk group in our dataset (Figure 3B). To validate these findings, we utilized the TCGA database (Figure 3C), and the results were consistent with those from our internal dataset. We also explored whether the risk-score system could distinguish the possibility of tumor metastasis and found that the proportion of patients with metastasis in the high-risk group was significantly higher than that in the low-risk group (Table 3, Figure 3D). We also analyzed the relationship between

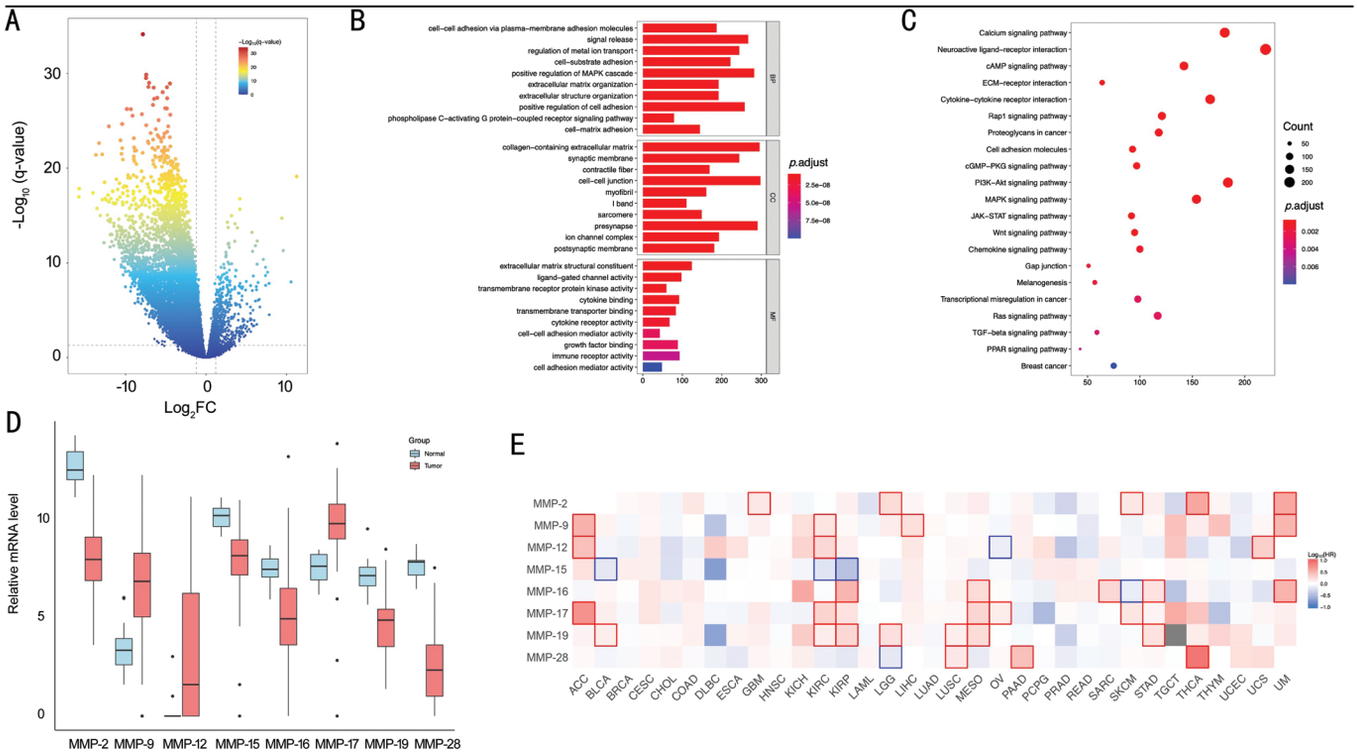


**Figure 1 DEGs between the normal choroid and UM** A: Volcano plot of DEGs between the normal choroid and UM; B: GO Enrichment bar plot of DEGs between normal choroid and UM; C: KEGG Enrichment dot plot of DEGs between the normal choroid and UM; D: Eight differentially expressed MMPs in normal choroid and UM tissues; E: Expression and prognostic correlation of eight differentially expressed MMPs across 33 types of tumors in TCGA database. ACC: Adrenocortical carcinoma; BLCA: Bladder urothelial carcinoma; BRCA: Breast invasive carcinoma; CESC: Cervical squamous cell carcinoma and endocervical adenocarcinoma; CHOL: Cholangiocarcinoma; COAD: Colon adenocarcinoma; DLBC: Diffuse large B-cell lymphoma; ESCA: Esophageal carcinoma; GBM: Glioblastoma multiforme; HNSC: Head and neck squamous cell carcinoma; KICH: Renal chromophobe cell carcinoma; KIRC: Renal clear cell carcinoma; KIRP: Renal papillary cell carcinoma; LAML: Acute myeloid leukemia; LGG: Brain low-grade glioma; LIHC: Liver hepatocellular carcinoma; LUAD: Lung adenocarcinoma; LUSC: Lung squamous cell carcinoma; MESO: Mesothelioma; OV: Ovarian serous cystadenocarcinoma; PAAD: Pancreatic adenocarcinoma; PCPG: Pheochromocytoma and paraganglioma; PRAD: Prostate adenocarcinoma; READ: Rectum adenocarcinoma; SARC: Sarcoma; SKCM: Skin cutaneous melanoma; STAD: Stomach adenocarcinoma; TGCT: Testicular germ cell tumors; THCA: Thyroid carcinoma; THYM: Thymoma; UCEC: Uterine corpus endometrial carcinoma; UCS: Uterine carcinosarcoma; UM: Uveal melanoma; DEGs: Differential expression genes; GO: Gene Ontology; KEGG: Kyoto Encyclopedia of Genes and Genomes; MMPs: Matrix metalloproteinases.

risk-score and pathology. Although there was no significant difference in risk-score between different pathological types of UM, higher scores were observed for epithelioid cell-type UM (Figure 3E). Then, we conducted GO and KEGG functional enrichment analyses on the DEGs between the high-risk and low-risk groups (Figure 3F-3G), as well as GSEA (Figure 3H). The results revealed that the majority of pathways were associated with the TME, such as cell-cell interaction and immune cell activation.

To verify the expression of MMPs in the two risk groups, we performed immunohistochemistry staining for MMP-2 and MMP-28 on UM tissues (Figure 4). We found that MMP-2 expression was significantly higher in the high-risk group compared to the low-risk group, while MMP-28 showed higher expression in low-risk group.

**Prognostic Prediction Models based on MMPs-related Risk-score System** To use risk-score more accurately to predict the prognosis of a large number of patients (rather than just dividing them into high-risk and low-risk groups), we used the risk-score alone to predict the prognosis of patients and found a higher proportion of deaths in the high-risk group compared to the low-risk group at first (Figure 5A). The 1-, 3- and 5-year prognosis prediction accuracy of risk-score alone was 81.8%, 78.8%, and 83.8%, respectively (Figure 5B). To enhance the comprehensive accuracy of the prognosis model, we constructed the Nomogram prognostic prediction model based on the risk-score system. Taking into account the conclusions of the large UM cohort study previously published by our team[5] and the results of Cox regression analysis of clinical characteristics and prognosis of 53 patients in this study (Table 4). In addition to the risk-score, we also included pathological type, tumor size, age, the largest basal diameter, tumor thickness and other clinical factors for Cox regression analysis. It was found that risk-score and pathological type

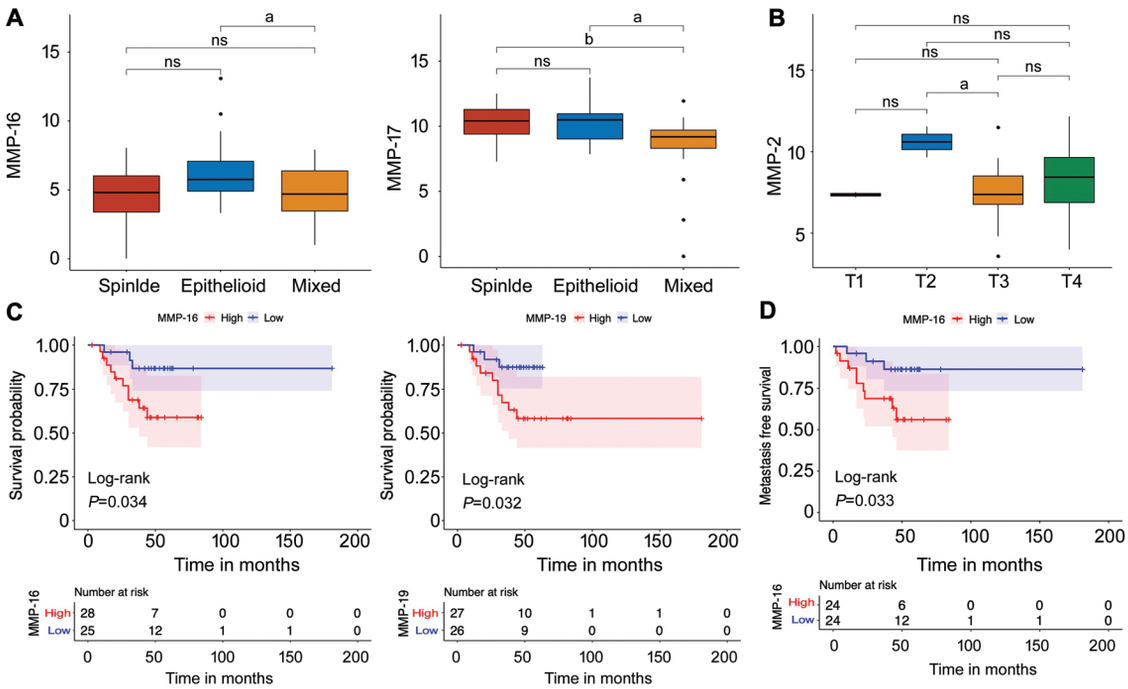


**Figure 2 Differentially expressed MMPs with traditional clinical prognostic risk factors and survival status** A: MMPs with statistically significant expression differences in UM pathological types; B: MMP with statistically significant expression difference in UM staging; C: MMPs whose expression levels are associated with survival status; D: MMP whose expression level is associated with metastatic status. UM: Uveal melanoma; MMPs: Matrix metalloproteinases. [a]*P*<0.05, [b]*P*<0.01.

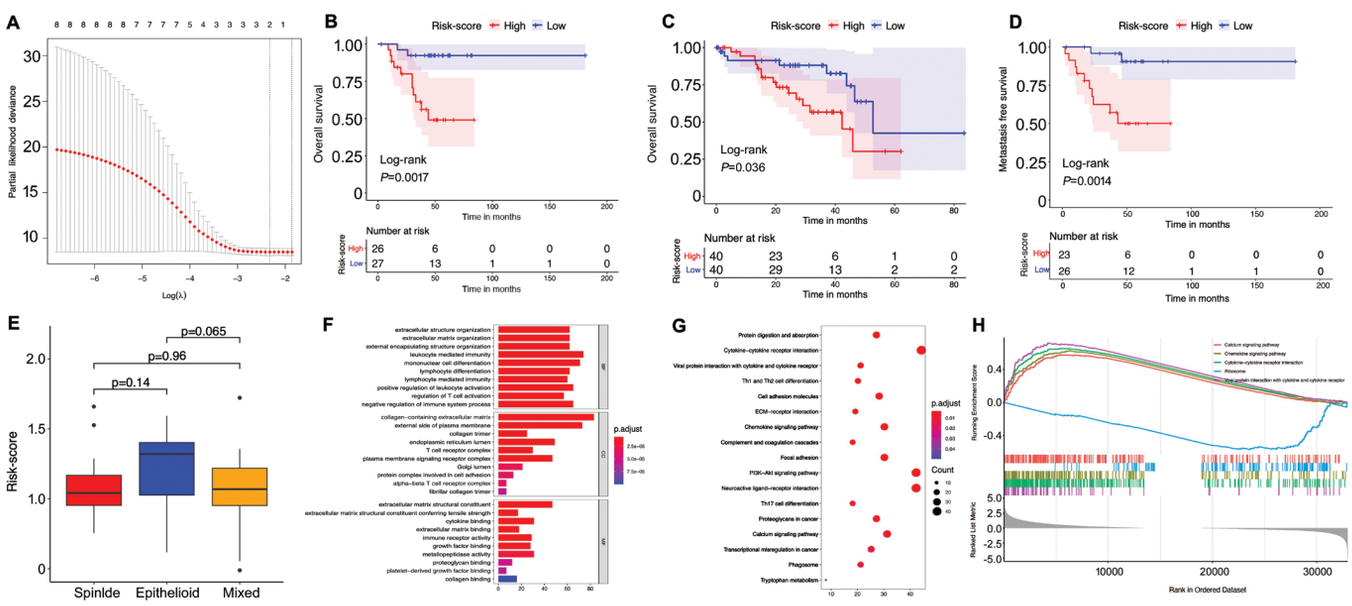


**Figure 3 Construction of MMPs-related risk-score system** A: LASSO regression curve, determining the optimal λ value as 2; B: Survival status of patients between high- and low-risk groups from our dataset; C: Survival status of 80 cases of UM patients from the TCGA database after grouping based on the risk-score system; D: Metastasis status of patients between two risk groups; E: The risk-score of different pathological types of UM; F: GO enrichment result of DEGs between the high-risk and low-risk groups; G: KEGG enrichment result of DEGs between the high-risk and low-risk groups; H: GSEA result between the high-risk and low-risk groups. UM: Uveal melanoma; DEGs: Differential expression genes; GO: Gene Ontology; KEGG: Kyoto Encyclopedia of Genes and Genomes; MMPs: Matrix metalloproteinases; GSEA: Gene Set Enrichment Analysis.

were independent prognostic factors of UM patients in this study (Figure 5C), so we used risk-score and pathological type to construct the Nomogram model for 1-, 3-, and 5-year overall survival (Figure 5D). The calibration curves showed that the 1-, 3-, and 5-year corrected curves were close to the ideal curve, indicating that the model's predictions align well with the actual outcomes (Figure 5E-5G). All of these findings suggested that this model effectively predicts patient prognosis.

**Table 2 Correlation between risk-score and clinicopathological features in UM**

| Parameters | High-risk | Low-risk | *P* |
|---|---|---|---|
| Gender, *n* (%) | | | 0.49 |
| Male | 11 (42.3) | 15 (57.7) | |
| Female | 15 (55.6) | 12 (44.4) | |
| Age (y), *n* (%) | | | 0.20 |
| 21-40 | 6 (42.9) | 8 (57.1) | |
| 41-60 | 13 (43.3) | 17 (56.7) | |
| 61-80 | 7 (77.8) | 2 (22.2) | |
| Laterality, *n* (%) | | | 1.0 |
| Right | 13 (48.2) | 14 (51.8) | |
| Left | 13 (50.0) | 13 (50.0) | |
| Intraocular pressure (mm Hg), *n* (%) | | | 0.56 |
| 10-21 | 22 (53.7) | 19 (46.3) | |
| <10 | 2 (40.0) | 3 (60.0) | |
| >21 | 2 (28.6) | 5 (71.4) | |
| Visual acuity, *n* (%) | | | 0.80 |
| >0.5 | 2 (50.0) | 2 (50.0) | |
| 0.1-0.5 | 4 (36.4) | 7 (63.6) | |
| <0.1 | 20 (52.6) | 18 (47.4) | |
| Largest basal diameter (mm) | 16.8±3.4 | 13.9±4.3 | 0.01 |
| Thickness (mm) | 11.65±2.4 | 10.8±2.8 | 0.26 |
| Size (T Stage)[a], *n* (%) | | | 0.04 |
| T1-T3 | 10 (34.5) | 19 (65.5) | |
| T4 | 16 (66.7) | 8 (33.3) | |
| Stage[a], *n* (%) | | | 0.18 |
| I-II | 6 (33.3) | 12 (66.7) | |
| III | 20 (57.1) | 15 (42.9) | |
| Macroscopic appearance, *n* (%) | | | 0.49 |
| Mushroom | 11 (42.3) | 15 (57.7) | |
| Hemisphere | 8 (50.0) | 8 (50.0) | |
| Irregular | 7 (63.6) | 4 (36.4) | |
| Optic disk involvement, *n* (%) | | | 0.42 |
| No | 24 (52.2) | 22 (47.8) | |
| Yes | 2 (28.6) | 5 (71.4) | |
| Subretinal fluid, *n* (%) | | | 1.0 |
| No | 1 (50.0) | 1 (50.0) | |
| Yes | 25 (49.0) | 26 (51.0) | |
| Intraocular hemorrhage, *n* (%) | | | 1.0 |
| No | 24 (50.0) | 24 (50.0) | |
| Yes | 2 (40.0) | 3 (60.0) | |
| Ciliary body involvement, *n* (%) | | | 0.89 |
| No | 13 (46.4) | 15 (53.6) | |
| Yes | 13 (52.0) | 12 (48.0) | |
| Extraocular extension, *n* (%) | | | 1.0 |
| No | 24 (49.0) | 25 (51.0) | |
| Yes | 2 (50.0) | 2 (50.0) | |
| Pathology, *n* (%) | | | 0.21 |
| Spindle cell-type | 7 (36.8) | 12 (63.2) | |
| Mixed cell-type | 10 (47.6) | 11 (52.4) | |
| Epithelioid cell-type | 9 (69.2) | 4 (30.8) | |

[a]American Joint Committee on Cancer classification (8th edition). UM: Uveal melanoma.

**Table 3 Different risk groups and the occurrence of metastasis**

| Risk group | Metastasis status | | Total | *P* |
|---|---|---|---|---|
| | Metastasis | Non-metastasis | | |
| High-risk | 13 | 13 | 26 | 0.003 |
| Low-risk | 3 | 24 | 27 | |
| Total | 16 | 37 | 53 | |

**Tumor Microenvironment and Immune Infiltrating Cells**

Since most of the DEGs between the high- and low-risk groups was concentrated in TME, we used the ESTIMATE algorithm to evaluate the stromal score, immune score, and tumor purity between the two groups based on the RNA sequencing results of 53 UM tissues. The results showed that ESTIMATE, immune, and stromal scores were higher in the high-risk group (Figure 6A), while tumor purity was higher in the low-risk group (Figure 6B). Subsequently, CIBERSORT was used to analyze immune cells in the TME (Figure 6C) and found that M1 macrophages and regulatory T cells were enriched in the high-risk group, while mast cells, monocytes, and CD4-positive T cells were enriched in the low-risk group (Figure 6D). Furthermore, compared to other immune cells, TAMs had the highest proportion in the TME, and their abundance was higher in the high-risk group (Figure 6E), and they are positively correlated with risk-score ($P$<0.001; Figure 6F). In addition, we also analyzed the correlation among 22 kinds of immune infiltrating cells. The results showed that the activated memory CD4-positive T cells were associated with memory B cells and plasma cells, while CD8-positive T cells were associated with regulatory T cells and mast cells (Figure 6G).

## DISCUSSION

Based on the largest transcriptome database of UM and choroidal tissues in Asia, we developed a machine learning model for predicting prognosis through MMPs and conducted a TME analysis. MMPs are a family of secreted neutral proteinases that can initiate the degradation of collagens and other ECM components and exert their effects through receptor-mediated interactions with neighboring cells[19]. MMPs can degrade intercellular adhesion molecules, disrupt the basement membrane, and facilitate tumor cell invasion into the ECM. By disrupting endothelial cells and the basement membrane of blood vessels, they assist tumor cells in entering and exiting the circulatory system. MMPs also activate growth factors constrained within the ECM and release active protein fragments, promoting the growth of distant micrometastases. As UM primarily metastasizes hematogenously, it can be anticipated that MMPs' degradation of ECM in tumor tissue would promote the distant metastasis of UM cells. MMPs not only participate in ECM destruction but also promote angiogenesis, EMT, and tumor cell migration[20]. There was a certain level of MMP-2 expression in normal choroid tissues, which has been proven necessary for developing

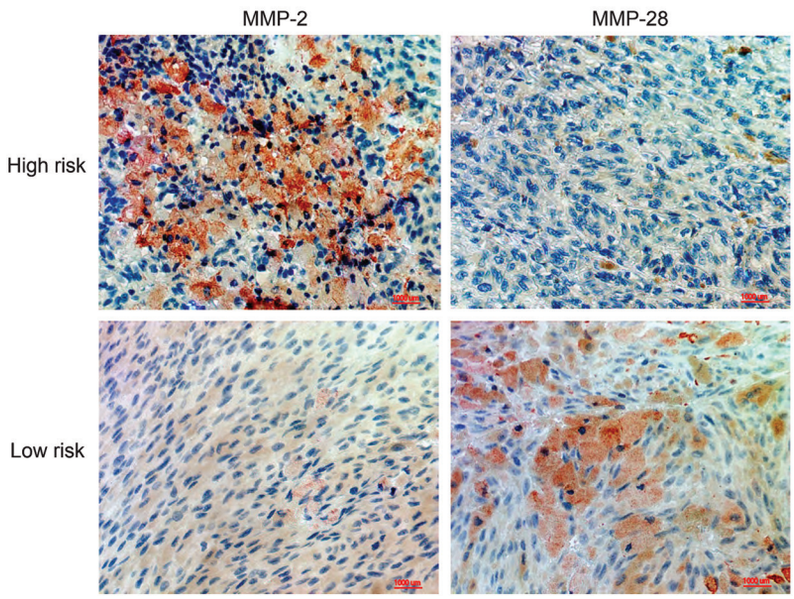


**Figure 4 Immunohistochemical staining of MMP-2 and MMP-28 in two risk groups** After depigmentation, the pigment granules appeared light brown. With 3-amino-9-ethylcarbazole staining, positive antibody showed as red. MMPs: Matrix metalloproteinases.

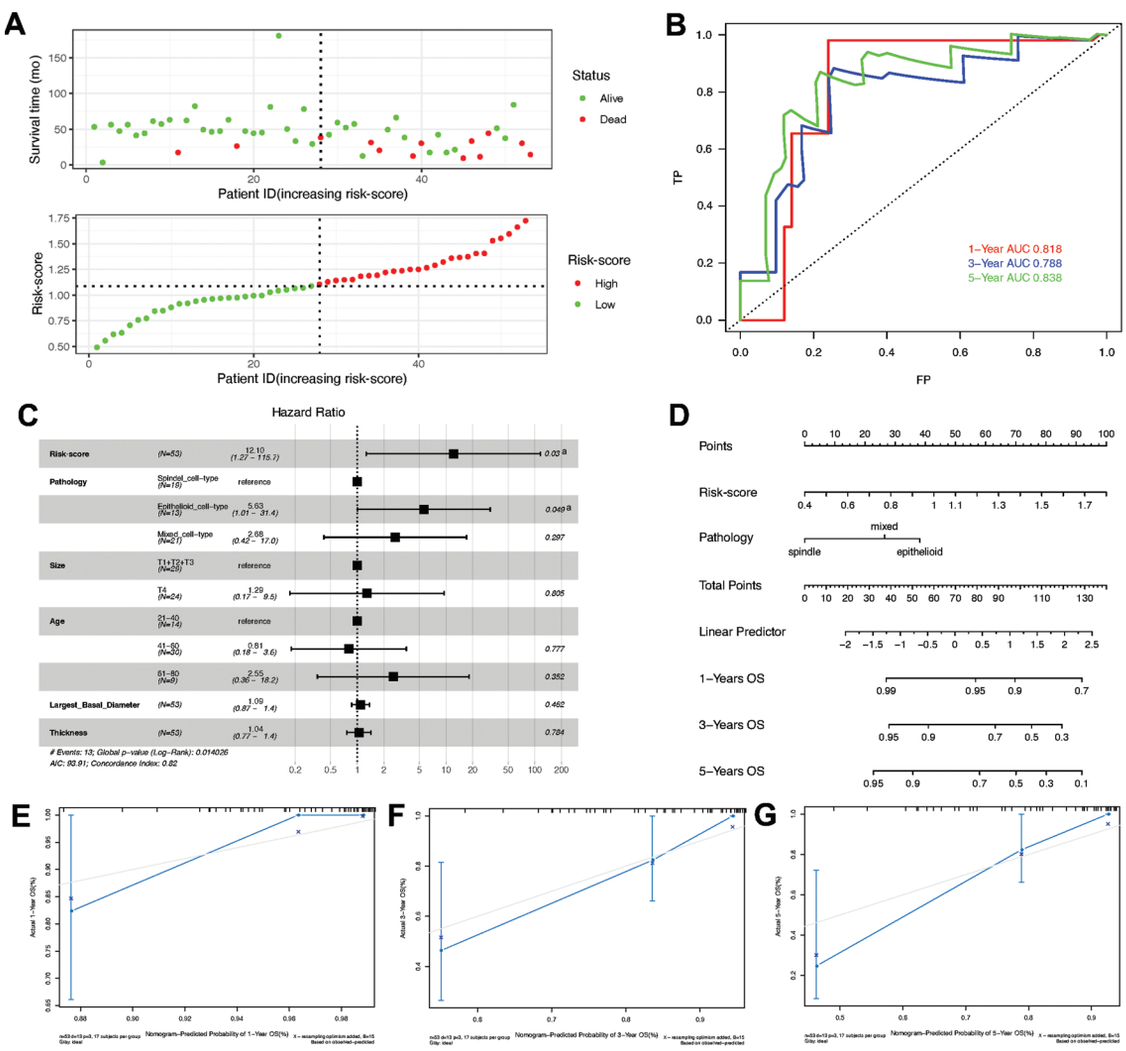


**Figure 5 MMPs-related prognosis prediction models** A: Patient's risk factor interaction plot for different risk-scores; B: ROC curves and AUC values after 1-, 3-, and 5-year diagnosis using only the risk-score; C: Forest plot of the multivariate Cox regression analysis for 53 UM patients; D: Nomogram model predicting 1-, 3-, and 5-year prognosis based on risk-score and pathological type; E-G: Calibration curve for predicting 1-,3-, and 5-year prognosis using the Nomogram model, respectively. MMPs: Matrix metalloproteinases; UM: Uveal melanoma; ROC: Receiver operating characteristic curve; AUC: Area under the curve. [a]*P*<0.05.

**Table 4 Univariate and multivariate analysis by Cox regression for UM-related metastasis and all causes of death**

| Parameters | UM-related metastasis (12 patients available) | | | | | All-causes death (13 patients available) | | | | |
|---|---|---|---|---|---|---|---|---|---|---|
| | Univariate analysis | | Multivariate analysis | | | Univariate analysis | | Multivariate analysis | | |
| | HR | *P* | HR | 95%CI | *P* | HR | *P* | HR | 95%CI | *P* |
| Gender | | | | | | | | | | |
| Male | Ref | - | | | | Ref | - | | | |
| Female | 1.04 | 0.95 | | | | 1.42 | 0.54 | | | |
| Age (y) | | | | | | | | | | |
| 21-40 | Ref | - | Ref | - | - | Ref | - | Ref | - | - |
| 41-60 | 1.70 | 0.50 | 1.22 | 0.20-7.61 | 0.83 | 1.22 | 0.77 | 0.98 | 0.23-4.20 | 0.98 |
| 61-80 | 2.33 | 0.40 | 3.26 | 0.34-31.69 | 0.31 | 2.95 | 0.19 | 3.91 | 0.61-25.13 | 0.15 |
| Laterality | | | | | | | | | | |
| Right | Ref | - | | | | Ref | - | | | |
| Left | 1.09 | 0.87 | | | | 1.74 | 0.33 | | | |
| Visual acuity | 0.21 | 0.39 | | | | 0.44 | 0.56 | | | |
| Intraocular pressure (mm Hg) | | | | | | | | | | |
| 10-21 | Ref | - | | | | Ref | - | | | |
| <10 | 0.81 | 0.85 | | | | 0.86 | 0.89 | | | |
| >21 | <0.001 | 0.99 | | | | 0.50 | 0.51 | | | |
| Largest basal diameter (mm) | 1.20 | 0.02 | 1.12 | 0.84-1.49 | 0.44 | 1.18 | 0.03 | 1.08 | 0.86-1.37 | 0.51 |
| Thickness (mm) | 1.06 | 0.58 | 0.99 | 0.74-1.30 | 0.92 | 1.15 | 0.21 | 1.05 | 0.77-1.42 | 0.77 |
| Size[a] | | | | | | | | | | |
| T1-T3 | Ref | - | Ref | - | - | Ref | - | Ref | - | - |
| T4 | 2.22 | 0.17 | 0.99 | 0.14-7.06 | 0.99 | 3.21 | 0.05 | 1.53 | 0.22-10.71 | 0.67 |
| Macroscopic appearance | | | | | | | | | | |
| Mushroom | Ref | - | Ref | - | - | Ref | - | | | |
| Hemisphere | 1.02 | 0.98 | 0.70 | 0.09-5.21 | 0.73 | 0.25 | 0.19 | | | |
| Irregular | 6.73 | 0.005 | 3.72 | 0.72-19.24 | 0.12 | 2.36 | 0.14 | | | |
| Optic disk involvement | | | | | | | | | | |
| No | Ref | - | | | | Ref | - | | | |
| Yes | 0.44 | 0.43 | | | | 0.45 | 0.44 | | | |
| Ciliary body involvement | | | | | | | | | | |
| No | Ref | - | | | | Ref | - | | | |
| Yes | 2.45 | 0.14 | | | | 2.79 | 0.09 | | | |
| Extraocular extension | | | | | | | | | | |
| No | Ref | - | | | | Ref | - | | | |
| Yes | 1.32 | 0.79 | | | | 1.02 | 0.98 | | | |
| Pathology | | | | | | | | | | |
| Spindle cell-type | Ref | - | Ref | - | - | Ref | - | Ref | - | - |
| Mixed cell-type | 2.69 | 0.23 | 1.40 | 0.17-11.33 | 0.75 | 2.29 | 0.34 | 2.62 | 0.40-17.23 | 0.32 |
| Epithelioid cell-type | 5.09 | 0.05 | 2.79 | 0.36-21.69 | 0.33 | 6.82 | 0.02 | 8.48 | 1.43-50.14 | 0.02 |

[a]American Joint Committee on Cancer classification (8th edition). HR: Hazard ratio; CI: Confidence interval; UM: Uveal melanoma.

and maintaining the vasculature[21]. However, the elevated expression of MMP-2 is a hallmark of multiple pathological situations, such as age-related macular degeneration and diabetic retinopathy[22-23]. Although there have been studies of MMPs in UM, there was scarce comparison with normal choroid tissues[24]. Additionally, due to the notably lower incidence of UM in the Asian population compared to Western countries, research on MMPs in Asian UM patients was limited, and most of them were based on qualitative studies (such as immunohistochemical staining)[9]. Therefore, our team included sequencing data from 17 normal choroid tissues and 53 UM tumor tissues to explore the impact of MMPs on UM prognosis more accurately.

MMP-2, one of the eight differentially expressed MMPs, exhibited a significant association with poor prognosis in patients, despite its lower expression in UM compared to the

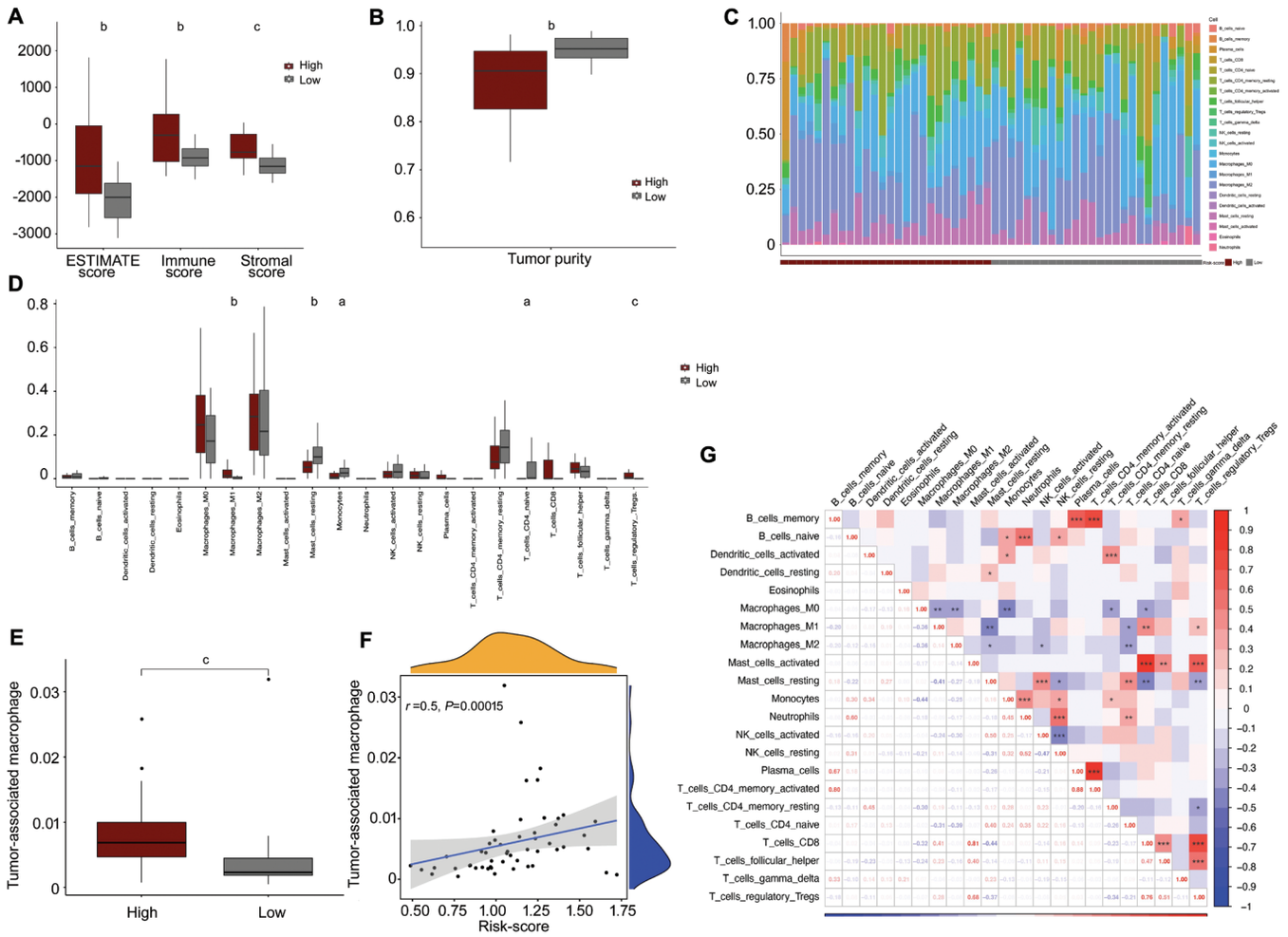


**Figure 6 Tumor microenvironment and immune infiltrating cells** A: Differences in ESTIMATE score, Stromal score, and Immune score between two groups; B: Differences in tumor purity between two groups; C: Distribution of 22 kinds of immune infiltrating cells in each UM sample; D: Differences in 22 types of immune infiltrating cells between two groups; E: Differences in TAMs between two groups; F: Relationship between TAMs and risk-score; G: Correlation between 22 types of immune infiltrating cells. UM: Uveal melanoma; TAMs: tumor-associated macrophages. [a]*P*<0.05, [b]*P*<0.01, [c]*P*<0.01.

normal group. This seems contradictory to the conventional notion that genes with low expression in tumors are associated with better prognosis. However, in our study, the control group consisted of choroid tissues from patients without ocular diseases, which have rich vasculature, and MMP-2 is predominantly expressed in endothelial cells within the choroid[25]. In contrast, most cells in UM tumor tissues are melanoma cells, with a small fraction of immune cells and a minimal number of endothelial cells[26-27]. In UM tissues, the expression levels of MMP-2 in vascular endothelial cells are significantly higher than in melanoma cells[28-29], which could explain why MMP-2's expression level is higher in normal choroid tissues compared to UM tissues. MMP-2 belongs to the collagenase subgroup of the MMPs family, and its overexpression can accelerate the degradation of ECM and vascular basement membrane, thereby promoting local invasion of tumor cells and their migration into blood vessels for metastasis[30]. Elshaw *et al*[31] found that all 10 UM tissues secreted MMP-2, with two UM samples secreting only MMP-2 showing stronger invasiveness. MMP-2 mainly promotes tumor cell invasion and metastasis by degrading ECM components such as type I and type IV collagen fibers and fibronectin. Besides ECM remodeling, EMT is also one of the ways MMP-2 influences tumor development. Studies have shown that the EMT process in UM tumor tissues promotes distant metastasis[32-33]. In our study, MMP-2 expression was positively correlated with risk-score, indicating that higher MMP-2 expression is associated with poorer prognosis in patients.

Compared with MMP-2, research on MMP-28 in tumors is relatively limited, and its correlation with prognosis varies in different types of cancers. In colon cancer[34] and Merkel cell carcinoma[35] (an invasive skin malignancy), MMP-28 seems to be associated with a lower degree of malignancy, consistent with our risk-score formula. However, in hepatocellular carcinoma[36] and pancreatic cancer[37], MMP-28 is associated

with poor prognosis. Therefore, the relationship between MMP-28 and the tumor's occurrence, development, and patient prognosis require further exploration.

According to the risk-score, we divided UM into high-risk and low-risk groups and statistically analyzed the clinical characteristics between the two groups (Table 2). It was found that the largest basal diameter and tumor size of the high-risk group were larger, and the previous articles published by our team also showed that the basal diameter was more closely related to the prognosis[5,38], which was consistent with Lai *et al*[28] found that MMP-2 was more strongly expressed at the edge of the tumor. Previous research has also suggested that MMP-2 can promote UM migration and invasion through various mechanisms[39], including the Wnt/β-Catenin and NF-κB pathways[40]. To validate whether the risk-score system based on MMP-2 and MMP-28 expression contributes to clinical prognosis, we analyzed patient follow-up records and found that the application of risk-score alone achieved an accuracy of approximately 80% in predicting the prognosis of UM at 1-, 3-, and 5-year after diagnosis (Figure 5B). This indicates that our risk-score can indeed reflect the degree of prognosis to a certain extent. In our study, although there was no statistically significant difference in the relationship between risk-score and different pathological types of UM, it was observed that the scores for epithelioid cell-type UM were higher than those for spindle and mixed cell-types. Cox multivariate analysis also found that risk-score and pathological types were associated with prognosis. To enhance the accuracy of predictions, we constructed a Nomogram prognosis prediction model (Figure 5D), which is composed of risk-score and pathological type. The predicted results were consistent with patients' actual prognosis, demonstrating our predictive model's effectiveness. Although the expression of MMP-16 was correlated with patient survival and metastatic status (*P*-values of 0.034 and 0.012, respectively), the risk-score system based on MMP-2 and MMP-28 demonstrated better discrimination of patient prognosis (*P*-values of 0.0017 and 0.0014, respectively), which means our MMPs-related risk-score system is more convincing in predicting prognosis than using single MMP. The UM patients who undergo local resection or enucleation surgery in our hospital often have excessively thick tumors or larger size. Previous studies have also found that patients with these kinds of tumors often have poor prognosis[41]. With the popularization of second-generation sequencing technology, evaluating the expression of MMPs in tumor tissues of UM patients undergoing local resection or enucleation, and predicting the risk of metastasis and death of UM based on our constructed MMPs-related prognostic prediction model, is helpful for clinical diagnosis and treatment and patient communication.

TME comprises cells and non-cellular components in tumor tissues, excluding tumor cells. Main components include fibroblasts, immune cells, endothelial cells, and the ECM[42]. In the high-risk group, the tumor stromal score and immune score were significantly higher than those in the low-risk group, which was consistent with the results of TME analysis of 80 UM samples from TCGA data by Tan *et al*[43]. Therefore, it can be inferred that the MMPs-related risk-score system indirectly reflects the role of TME in the invasion, migration, and metastasis processes of UM tumors. In this study, CD4-positive T cells in the low-risk group were significantly higher than in the high-risk group, aligning with the anti-tumor role of CD4-positive T cells observed in cutaneous melanoma[44] and glioblastoma[45]. TAMs are macrophages present in specific tumor pathological environments. In some tumors, markers traditionally classified as M1 and M2 macrophages can be co-expressed in individual macrophages in the TME[46], and some macrophages with high expression of M2-like TAMs markers are similar to M1-like TAMs in function[47]. It is speculated that TAMs are regulated by cancer cells, transforming them into macrophages with different functions. The functional diversity of TAMs in the TME may also vary depending on their location[48]. In this study, it is evident that the number of TAMs in UM is in absolute dominance among immune infiltrating cells (Figure 6D), and there are more TAMs in the high-risk group (Figure 6E). Mäkitie *et al*[49] also found that tumors with a higher concentration of TAMs had more UM patients who died due to metastasis. Previous studies have indicated that TAMs can promote the expression of the MMP family (including MMP-2), regulate Toll-like receptor signaling pathways, and enhance tumor invasion and metastasis[50-51]. Furthermore, TAMs-induced MMPs are also involved in promoting tumor angiogenesis[52]. Since UM primarily undergoes distant metastasis through the circulatory system[53], and MMP-2 is highly expressed in endothelial cells of UM[28], it is worth further experimental validation whether TAMs can promote UM vascular generation through MMPs, leading to metastasis. As the therapeutic effect of immune checkpoint inhibitors in patients with UM is not as good as that in patients with cutaneous melanoma, it is particularly important to explore clinical treatments for other immune cells in TME.

Our study also has some limitations. As a malignant tumor in the eye, UM has a minimal volume compared to tumors in other organs, such as liver cancer or breast cancer. Although our UM tissues were obtained from completely excised tumors after local resection or enucleation surgery, there are few surplus tissues for transcriptome sequencing after pathological examination, resulting in a smaller sample size due to the instability of RNA and the need for quality control. Therefore, only 53 cases of UM were included in this study. Even so, we

have successfully constructed a prognosis prediction model based on MMPs, which could be considered to complement AJCC staging and enhance the personalized diagnosis and treatment of patients. Moreover, while transcriptome sequencing includes cells other than cancer cells in tumor tissues and can infer the composition of the TME through bioinformatics analysis, it still cannot provide information on the differential distribution and function of cells in different tumor regions. However, based on the transcriptome sequencing results, we can roughly understand the impact of various cells in UM tissues on prognosis, such as the mentioned TAMs. Therefore, our team has begun to explore the heterogeneity of UM more precisely through single-cell sequencing and spatial transcriptomics.

In conclusion, this study conducted a comparative analysis of transcriptome sequencing between normal choroid tissue and UM tissue with the largest sample number in Asia. Based on the sequencing results from this database, along with corresponding clinical information and follow-up results of the patients, we constructed a risk-score system by machine learning based on MMP-2 and MMP-28 and related prognostic prediction models. Combining the advantages of transcriptome sequencing, we performed bioinformatics analysis on the TME of UM. The findings revealed that patients in the high-risk group had poorer clinical prognosis, higher tumor stromal scores, higher immune scores, and a correlation with TAMs and regulatory T cells enrichment.

## ACKNOWLEDGEMENTS

**Authors' Contributions:** Li Y and Wei WB had full access to all of the data in the study and took responsibility for the integrity of the data and the accuracy of the data analysis. Chen YN and Wei WB made contributed to concept and design, Chen YN, Xiu JY, Zhao HQ, and Luo JT contributed to acquisition, analysis, or interpretation of data. Yang Q, Li Y, and Wei WB contributed to funding acquisition, project administration, supervision, and review. All authors read and approved the final manuscript.

**Availability of Data and Materials:** Raw data of all normal choroid and UM samples were successfully uploaded on NCBI database and the data will be released at https://www.ncbi.nlm.nih.gov/sra/PRINA1091159 with publication. The datasets used and analyzed during the current study are available from the corresponding author on reasonable request. Researchers who require data from this study for research purposes can use it after obtaining the consent of the corresponding author (Wei WB, weiwenbintr@163.com) and signing a data access agreement.

**Foundations:** Supported by the National Natural Science Foundation of China (No.82220108017; No.82141128; No.82101180); Beijing Natural Science Foundation (No. Z220012); The Capital Health Research and Development of Special (No.2020-1-2052); Science & Technology Project of Beijing Municipal Science & Technology Commission (No.Z201100005520045); Sanming Project of Medicine in Shenzhen (No.SZSM202311018); Beijing Science & Technology Development of TCM (No.BJZYYB-2023-17).

**Conflicts of Interest: Chen YN,** None; **Xiu JY,** None; **Zhao HQ,** None; **Luo JT,** None; **Yang Q,** None; **Li Y,** None; **Wei WB,** None.

## REFERENCES

1 Singh AD, Turell ME, Topham AK. Uveal melanoma: trends in incidence, treatment, and survival. *Ophthalmology* 2011;118(9):1881-1885.

2 Park SJ, Oh CM, Kim BW, *et al*. Nationwide incidence of ocular melanoma in south Korea by using the national cancer registry database (1999-2011). *Invest Ophthalmol Vis Sci* 2015;56(8):4719.

3 Collaborative Ocular Melanoma Study Group. The COMS randomized trial of iodine 125 brachytherapy for choroidal melanoma: V. Twelve-year mortality rates and prognostic factors: COMS report No. 28. *Arch Ophthalmol* 2006;124(12):1684-1693.

4 Caminal JM, Mejia K, Masuet-Aumatell C, *et al*. Endoresection versus iodine-125 plaque brachytherapy for the treatment of choroidal melanoma. *Am J Ophthalmol* 2013;156(2):334-342.e1.

5 Chen YN, Wang YN, Chen MX, *et al*. Machine learning models for outcome prediction of Chinese uveal melanoma patients: a 15-year follow-up study. *Cancer Commun* (*Lond*) 2022;42(3):273-276.

6 Kessenbrock K, Plaks V, Werb Z. Matrix metalloproteinases: regulators of the tumor microenvironment. *Cell* 2010;141(1):52-67.

7 Villanueva J, Herlyn M. Melanoma and the tumor microenvironment. *Curr Oncol Rep* 2008;10(5):439-446.

8 Fu Y, Xiao W, Mao Y. Recent advances and challenges in uveal melanoma immunotherapy. *Cancers* (*Basel*) 2022;14(13):3094.

9 El-Shabrawi Y, Ardjomand N, Radner H, *et al*. MMP-9 is predominantly expressed in epithelioid and not spindle cell uveal melanoma. *J Pathol* 2001;194(2):201-206.

10 Gu C, Gu X, Wang Y, *et al*. Construction and validation of a novel immunosignature for overall survival in uveal melanoma. *Front Cell Dev Biol* 2021;9:710558.

11 Robertson AG, Shih J, Yau C, *et al*. Integrative analysis identifies four molecular and clinical subsets in uveal melanoma. *Cancer Cell* 2017;32(2):204-220.e15.

12 Ritchie ME, Phipson B, Wu D, *et al*. Limma powers differential expression analyses for RNA-sequencing and microarray studies. *Nucleic Acids Res* 2015;43(7):e47.

13 Yu G, Wang LG, Han Y, *et al*. clusterProfiler: an R package for comparing biological themes among gene clusters. *OMICS* 2012;16(5):284-287.

14 Tang Z, Kang B, Li C, *et al*. GEPIA2: an enhanced web server for large-scale expression profiling and interactive analysis. *Nucleic Acids Res* 2019;47(W1):W556-W560.

15 Friedman J, Hastie T, Tibshirani R. Regularization paths for generalized linear models *via* coordinate descent. *J Stat Softw* 2010;33(1):1-22.

16 Newman AM, Liu CL, Green MR, *et al*. Robust enumeration of cell subsets from tissue expression profiles. *Nat Methods* 2015;12(5):453-457.

17 Racle J, de Jonge K, Baumgaertner P, *et al*. Simultaneous enumeration of cancer and immune cell types from bulk tumor gene expression data. *eLife* 2017;6:e26476.

18 Quintero-Fabián S, Arreola R, Becerril-Villanueva E, *et al*. Role of matrix metalloproteinases in angiogenesis and cancer. *Front Oncol* 2019;9:1370.

19 Gialeli C, Theocharis AD, Karamanos NK. Roles of matrix metalloproteinases in cancer progression and their pharmacological targeting. *FEBS J* 2011;278(1):16-27.

20 Cabral-Pacheco GA, Garza-Veloz I, Castruita-De la Rosa C, *et al*. The roles of matrix metalloproteinases and their inhibitors in human diseases. *Int J Mol Sci* 2020;21(24):9739.

21 Summers JA. The choroid as a sclera growth regulator. *Exp Eye Res* 2013;114:120-127.

22 Wu W, Su Y, Hu C, Tao H, Jiang Y, Zhu G, Zhu J, Zhai Y, Qu J, Zhou X, Zhao F. Hypoxia-induced scleral HIF-2α upregulation contributes to rises in MMP-2 expression and myopia development in mice. *Invest Ophthalmol Vis Sci* 2022;63(8):2.

23 Pai HL, Hsieh SM, Su YS, *et al*. Short-term hyperuricemia leads to structural retinal changes that can be reversed by serum uric acid lowering agents in mice. *Invest Ophthalmol Vis Sci* 2022;63(10):8.

24 Wang T, Zhang Y, Bai J, *et al*. MMP1 and MMP9 are potential prognostic biomarkers and targets for uveal melanoma. *BMC Cancer* 2021;21(1):1068.

25 Kvanta A, Shen WY, Sarman S, *et al*. Matrix metalloproteinase (MMP) expression in experimental choroidal neovascularization. *Curr Eye Res* 2000;21(3):684-690.

26 Durante MA, Rodriguez DA, Kurtenbach S, *et al*. Single-cell analysis reveals new evolutionary complexity in uveal melanoma. *Nat Commun* 2020;11:496.

27 Li K, Sun L, Wang Y, *et al*. Single-cell characterization of macrophages in uveal melanoma uncovers transcriptionally heterogeneous subsets conferring poor prognosis and aggressive behavior. *Exp Mol Med* 2023;55(11):2433-2444.

28 Lai K, Conway RM, Crouch R, *et al*. Expression and distribution of MMPs and TIMPs in human uveal melanoma. *Exp Eye Res* 2008;86(6):936-941.

29 Väisänen A, Kallioinen M, von Dickhoff K, *et al*. Matrix metalloproteinase-2 (MMP-2) immunoreactive protein—a new prognostic marker in uveal melanoma? *J Pathol* 1999;188(1):56-62.

30 Stetler-Stevenson WG. The role of matrix metalloproteinases in tumor invasion, metastasis, and angiogenesis. *Surg Oncol Clin N Am* 2001;10(2):383-392,x.

31 Elshaw SR, Sisley K, Cross N, *et al*. A comparison of ocular melanocyte and uveal melanoma cell invasion and the implication of alpha1beta1, alpha4beta1 and alpha6beta1 integrins. *Br J Ophthalmol* 2001;85(6):732-738.

32 Neo SY, Oliveira MMS, Tong L, *et al*. Natural killer cells drive 4-1BBL positive uveal melanoma towards EMT and metastatic disease. *J Exp Clin Cancer Res* 2024;43(1):13.

33 Asnaghi L, Gezgin G, Tripathy A, *et al*. EMT-associated factors promote invasive properties of uveal melanoma cells. *Mol Vis* 2015;21:919-929.

34 Bister VO, Salmela MT, Karjalainen-Lindsberg ML, *et al*. Differential expression of three matrix metalloproteinases, MMP-19, MMP-26, and MMP-28, in normal and inflamed intestine and colon cancer. *Dig Dis Sci* 2004;49(4):653-661.

35 Suomela S, Koljonen V, Skoog T, *et al*. Expression of MMP-10, MMP-21, MMP-26, and MMP-28 in merkel cell carcinoma. *Virchows Arch* 2009;455(6):495-503.

36 Zhou J, Zheng X, Feng M, *et al*. Upregulated MMP28 in hepatocellular carcinoma promotes metastasis *via* Notch3 signaling and predicts unfavorable prognosis. *Int J Biol Sci* 2019;15(4):812-825.

37 Luan H, Jian L, Huang Y, *et al*. Identification of novel therapeutic target and prognostic biomarker in matrix metalloproteinase gene family in pancreatic cancer. *Sci Rep* 2023;13:17211.

38 Luo J, Chen Y, Yang Y, *et al*. Prognosis prediction of uveal melanoma after plaque brachytherapy based on ultrasound with machine learning. *Front Med* (*Lausanne*) 2021;8:777142.

39 Hou Q, Han S, Yang L, *et al*. The interplay of microRNA-34a, LGR4, EMT-associated factors, and MMP2 in regulating uveal melanoma cells. *Invest Ophthalmol Vis Sci* 2019;60(13):4503.

40 Zhao G, Yin Y, Zhao B. miR-140-5p is negatively correlated with proliferation, invasion, and tumorigenesis in malignant melanoma by targeting SOX4 *via* the Wnt/β-catenin and NF-κB cascades. *J Cell Physiol* 2020;235(3):2161-2170.

41 Shields CL. Metastasis of uveal melanoma millimeter-by-millimeter in 8033 consecutive eyes. *Arch Ophthalmol* 2009;127(8):989-998.

42 Xiao Y, Yu D. Tumor microenvironment as a therapeutic target in cancer. *Pharmacol Ther* 2021;221:107753.

43 Tan Y, Pan J, Deng Z, *et al*. Monoacylglycerol lipase regulates macrophage polarization and cancer progression in uveal melanoma and pan-cancer. *Front Immunol* 2023;14:1161960.

44 Bawden EG, Wagner T, Schröder J, *et al*. $CD4^+$ T cell immunity against cutaneous melanoma encompasses multifaceted MHC II–dependent responses. *Sci Immunol* 2024;9(91):eadi9517.

45 Zheng J, Wang L, Zhao S, *et al*. TREM2 mediates MHCII-associated $CD4^+$ T-cell response against gliomas. *Neuro Oncol* 2024;26(5):811-825.

46 Chong BF, Tseng LC, Hosler GA, *et al*. A subset of $CD163^+$ macrophages displays mixed polarizations in discoid lupus skin. *Arthritis Res Ther* 2015;17:324.

47 Elliott LA, Doherty GA, Sheahan K, *et al*. Human tumor-infiltrating myeloid cells: phenotypic and functional diversity. *Front Immunol* 2017;8:86.

48 Yang M, McKay D, Pollard JW, *et al*. Diverse functions of macrophages in different tumor microenvironments. *Cancer Res* 2018;78(19):5492-5503.

49 Mäkitie T, Summanen P, Tarkkanen A, *et al*. Tumor-infiltrating macrophages ($CD68^+$ cells) and prognosis in malignant uveal melanoma. *Invest Ophthalmol Vis Sci* 2001;42(7):1414-1421.

50 Ke X, Zhang S, Wu M, *et al*. Tumor-associated macrophages promote invasion *via* Toll-like receptors signaling in patients with ovarian cancer. *Int Immunopharmacol* 2016;40:184-195.

51 Zhu X, Liang R, Lan T, *et al*. Tumor-associated macrophage-specific CD155 contributes to M2-phenotype transition, immunosuppression, and tumor progression in colorectal cancer. *J Immunother Cancer* 2022;10(9):e004219.

52 Fu LQ, Du WL, Cai MH, *et al*. The roles of tumor-associated macrophages in tumor angiogenesis and metastasis. *Cell Immunol* 2020;353:104119.

53 Jager MJ, Shields CL, Cebulla CM, *et al*. Uveal melanoma. *Nat Rev Dis Primers* 2020;6:24.